Solution of temperature field in DC cast aluminium alloy billet by the dual reciprocity boundary element method

Božidar Šarler and Jure Mencinger
Laboratory for Fluid Dynamics and Thermodynamics, Faculty of Mechanical Engineering, University of Ljubljana, Slovenia

Received February 1998
Revised August 1998
Accepted October 1998

Keywords *Alloys, Boundary element method, Castings, Convective-diffusive problems, Phase change, Spline function*

Abstract *The axisymmetric steady-state convective-diffusive thermal field problem associated with direct-chill, semi-continuously cast billets has been solved using the dual reciprocity boundary element method. The solution is based on a formulation which incorporates the one-phase physical model, Laplace equation fundamental solution weighting, and scaled augmented thin plate splines for transforming the domain integrals into a finite series of boundary integrals. Realistic non-linear boundary conditions and temperature variation of all material properties are included. The solution is verified by comparison with the results of the classical finite volume method. Results for a 0.500 [m] diameter Al 4.5 per cent Cu alloy billet at typical casting conditions are given.*

Nomenclature

c	= specific heat of the contiuum	h_{err}	= prescribed iteration error
$c_{p\mathcal{P}}$	= specific heat at constant pressure of phase $\mathcal{P}$	h_{steady}	= prescribed error for steady-state determination
c_{pw}	= specific heat of water	$\mathbf{H}$	= fundamental flux matrix
c_{ϖ}	= material property underrelaxation factor	$\mathcal{H}_{\Gamma}$	= heat transfer coefficient (on the boundary)
c^*	= fundamental solution geometry coefficient	$\mathcal{H}_{\Gamma\mathrm{high}}$	= constant in mould heat transfer coefficient correlation
E	= complete elliptic integral of the second kind	$\mathcal{H}_{\Gamma\mathrm{low}}$	= constant in mould heat transfer coefficient correlation
$f_{\mathcal{P}}$	= temperature dependent volume fraction	$\mathcal{I}_1$	= weighting integral of the transience and source terms
F_{Γ}	= known heat flux on the boundary	$\mathcal{I}_2$	= weighting integral of the convection term
$\mathbf{F}_{\mathcal{P}}$	= heat flux of phase $\mathcal{P}$	$\mathcal{I}_3$	= weighting integral of the diffusion term
$\mathcal{F}$	= arbitrary scalar valued function	k	= thermal conductivity of the continuum
$\boldsymbol{\mathcal{F}}$	= vector with scalars $\mathcal{F}_i$	$k_{\mathcal{P}}$	= thermal conductivity of phase $\mathcal{P}$
$\boldsymbol{\mathcal{G}}$	= arbitrary vector valued function	k_0	= representative thermal conductivity
$\mathbf{G}$	= fundamental solution matrix	K	= complete elliptic integral of the first kind
$h_{\mathcal{M}}$	= specific latent heat of the solid-liquid phase change	$\mathbf{n}_{\Gamma}(\mathbf{p})$	= outward pointing normal on Γ
$h_{\mathcal{P}}$	= specific enthalpy of phase $\mathcal{P}$		
$h_{\mathcal{LS}}$	= enthalpy difference		

The authors would like to acknowledge the Ministry of Science and Technology of the Republic of Slovenia for support in the framework of the projects Two-element modelling of solidification and COST-512: Modelling in materials science and processing. The DC casting model was developed for the aluminium company IMPOL Slovenska Bistrica, Slovenia. The authors are grateful to the management of the company for allowing the publication of the present results.

N = number of mesh points
N_Γ = number of mesh points on the boundary and number of boundary elements
N_Ω = number of mesh points in the domain
N_Ψ = number of global interpolation functions
$\mathbf{p}$ = field point position vector
Q = billet coolant flow
r = Euclidean distance between field and collocation point
r = radial coordinate
r_s = radial coordinate of the source point
r_n = radial coordinate of the shape function Ψ_n
r_0 = reference radial coordinate
$r_{\max}$ = billet radius
$\mathbf{s}$ = source point position vector
t = time
t_0 = initial time
T = temperature
T_S = solidus temperature
$T_\mathcal{L}$ = liquidus temperature
$T_\mathcal{M}$ = mean phase change temperature
$T_{\mathcal{LS}}$ = phase change interval
T_h = enthalpy reference temperature
$T(\mathbf{p}, t_0)$ = initial temperature
T_Γ = known temperature on the boundary
$T^*(\mathbf{p};\mathbf{s})$ = fundamental solution of the Laplace equation
$T_\mathcal{T}$ = Kirchhoff variable reference temperature
T_Γ = billet boundary temperature
$T_{\Gamma\text{ref}}$ = bulk cooling water temperature
$\bar{T}$ = mean temperature $\bar{T} = \frac{1}{2}(T_\Gamma + T_{\Gamma\text{ref}})$
$\mathcal{T}(T)$ = Kirchhoff variable
$\mathbf{v}P$ = velocity of the phase $\mathcal{P}$
z = axial coordinate
z_s = axial coordinate of the source point
z_n = axial coordinate of the shape function Ψ_n
z_0 = reference axial coordinate

Greek symbols

Γ = boundary
Γ^D = boundary with Dirichlet type boundary conditions
Γ^N = boundary with Neumann type boundary conditions
Γ^R = boundary with Robin type boundary conditions
Δt = positive time increment
Δz = positive increment of the axial coordinate
ι = coefficient of implicitness
ϖ = arbitrary temperature-dependent quantity
ρ = first modified distance between field and source point
ρ_n = first modified distance between field and collocation point
$\tilde{\rho}$ = second modified distance between field and source point
$\tilde{\rho}_n$ = second modified distance between field and collocation point
$\varrho_\mathcal{P}$ = temperature dependent density
ϱ_0 = representative density
ϱ_W = density of water
ς_u = shape function coefficient
$\boldsymbol{\varsigma}$ = vector with shape function coefficient ς_u
$\boldsymbol{\Phi}$ = abbreviation in convection term
$\psi_u(\mathbf{p})$ = global interpolation function
$\hat{\psi}_u(\mathbf{p})$ = harmonic global interpolation function
$\boldsymbol{\Psi}$ = shape function geometry matrix
Ω = connected fixed domain

Superscripts

j = timestep counter
m = iteration counter

1. Introduction

The BEM (Brebbia *et al.*, 1984) is a weighted residual method for solving partial differential equations, characterized by choosing an appropriate fundamental solution as a weighting function and by using the generalized Green's formula for complete transfer of one or more partial differential operators on the weighting function. The main comparative advantage of the boundary element method over other discrete approximative methods is demonstrated in cases where this procedure results solely in a boundary integral equation. This turns out to be possible only for some partial differential equations. In general the procedure results in a boundary-domain integral equation. The former and the latter cases are demonstrated by two examples. The first one deals with the boundary element method for the Laplace equation, structured with the fundamental solution of the Laplace equation (steady diffusion) – the procedure results in boundary-only formulation. The second one deals with the boundary element method for the general transport equation (transient convection-

diffusion) structured by weighting with the fundamental solution of the Laplace equation – the domain integrals appear at least from the transience, convection, and source terms.

The numerical solution of the boundary integral equations is very effective since the discretization of the fields and geometry is concentrated on the boundary alone. The numerical solution of boundary-domain integral equations is less effective since in addition to the boundary discretization into boundary elements, the domain has to be discretized into domain cells. The numerical solution of the resulting boundary or boundary-domain integrals turns out to be very accurate also for the most basic piece-wise constant order of discretization. However, the domain cell discretization makes the method very similar to the classical Finite Element (FEM) or Finite Volume Methods (FVM) and with this the principal attraction of the BEM seems to be lost.

One of the possibilities for treating the resultant domain integrals with a finite series of boundary integrals instead of the domain cells is the Dual Reciprocity Boundary Element Method (DRBEM) (Partridge *et al.*, 1992). The key point of the DRBEM is approximation of the field in the domain by a set of global approximation functions and subsequent representation of the domain integrals of these global approximation functions by the boundary integrals. In DRBEM all calculations reduce to evaluation of the boundary integrals only. Despite the proved practical applicability of the DRBEM (Aliabadi *et al.*, 1995), important theoretical questions remain. For example, which global interpolation functions are most suitable for representation of the fields in the domain, and where should the collocation points of these global interpolation functions be put? Up to present, both questions have been addressed mostly from the heuristic point of view. The most popular global interpolation function used in the majority of the DRBEM calculations so far in the field of transport phenomena is $1 + r$, with r representing the Euclidean distance between field and collocation point. The convergence of these functions was studied both numerically and in a more formal way in Yamada *et al.* (1994). Up to now, only *ad-hoc* distributed collocation points have been used, since an appropriate error estimator does not exist.

Some mathematically substantiated answers to the first question have been recently rediscovered by Golberg and Chen in works concerning the theory of radial basis functions (Golberg and Chen, 1994). It has been demonstrated (Duchon, 1997) that the use of thin plate spline radial basis functions gives an approximation in which the curvature is minimized. The first theoretical investigations of the convergence of these functions were carried out in (Buhmann, 1990). An error and convergence analysis for the DRBEM for the Poisson equation have been recently reported by Golberg *et al.* (1998).

The global interpolation of the fields over a domain introduces unknowns in the domain in addition to the unknowns at the boundary. The number of these additional unknowns usually exceeds the number of boundary unknowns. The systems of algebraic equations resulting from DRBEM are thus large, fully populated and asymmetric. A third important but not sufficiently investigated

element of the DRBEM method is the possible iterative solution of associated systems of algebraic equations. This issue is of utmost importance when solving large-scale problems. Bulgakov *et al.* (1998) recently propose two iterative solution techniques for DRBEM matrices originating from the diffusion equation.

The DRBEM for solving the energy transport equation was first applied to simple diffusion-governed linear (Wrobel *et al.*, 1986) and nonlinear problems (Wrobel and Brebbia, 1987), then to steady-state convective-diffusive problems (Partridge *et al.*, 1992), and finally successfully demonstrated in a fixed grid (one-domain) completely non-linear transient convective-diffusive context including phase-change effects and nonlinearities arising simultaneously from material properties and boundary conditions (Šarler and Kuhn, 1998a; Šarler and Kuhn, 1998b). This development upgrades the DRBEM method for solving problems previously exclusively coped with by using more established numerical approaches. A comprehensive review of attempts to use boundary element methods in micro- and macroscopic melting and solidification problems can be found in Šarler *et al.* (1993).

Direct-Chill (DC) casting is currently the most common semi-continuous casting practice in non-ferrous metallurgy (Emley, 1976). The process involves molten metal being fed through a bottomless water-cooled mould where it is sufficiently solidified around the outer surface that it takes the shape of the mould and acquires sufficient mechanical strength to contain the molten core at the centre. As the ingot emerges from the mould, water impinges directly from the mould onto the ingot surface (direct-chill), falls over the cast surface and completes the solidification. A schematic of the process is given in Figure 1.

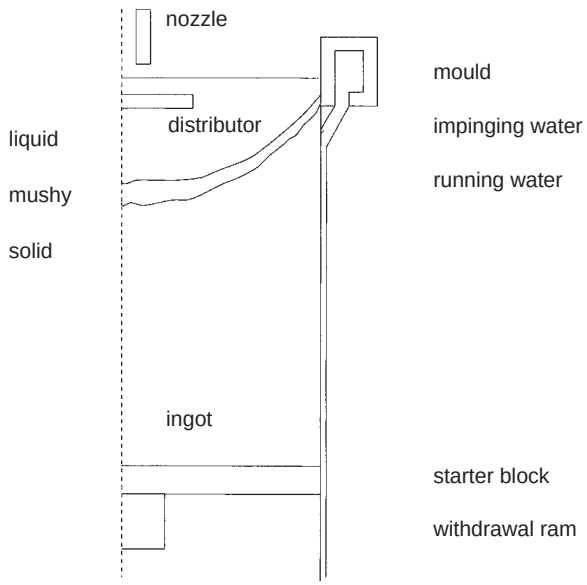

Figure 1.
Schematics of the DC casting process

Related transport, solid-mechanics, and phase-change kinetics phenomena (Katgerman *et al.*, 1990) have been extensively studied and many different numerical methods have been used to solve the respective DC casting models.

The proper prediction of the temperature, velocity, concentration and phase fields in the ingot is one of the prerequisites for optimization of the process with respect to its quality and productivity. State-of-the-art models of the process (Reddy and Beckermann, 1997) are partially based on the one-phase (Voller *et al.*, 1989) and partially on the two-phase formulation (Ni and Beckermann, 1991) of the binary eutectic solid-liquid phase change system, and the computational model at least qualitatively corresponds to the measurements.

Up to now, the BEM has been used only for dealing with physically much simpler DC casting situations. Very recently, Bialecki *et al.* (1996) proposed a two-dimensional front tracking (two-domain) boundary integral formulation solution of the continuous casting problem structured through the steady convective-diffusive fundamental solution weighting. The resultant extremely efficient boundary only method is particularly suitable in rough inverse modelling estimates (Nowak *et al.*, 1996). However, its main restrictions are the constant thermal properties of the phases, the uniform velocity field, and the lack of being able to cope with materials solidifying over a temperature range.

This paper demonstrates the use of the newly proposed dual reciprocity boundary element technique (Šarler, 1996) for solving a wide range of continuous casting problems without the aforementioned limitations. It is based on the fixed-grid (one-domain) formulation structured with the fundamental solution of the Laplace equation and scaled thin plate spline global interpolation functions. The present work upgrades the previous use of the dual reciprocity method in an axisymmetric heat transfer context (Wrobel and Telles, 1996) in many ways. The inclusion of the convection term, treatment of the phase-change, provision for temperature dependent material properties and use of the axisymmetric form of the scaled thin plate splines which replace the previously used heuristic global interpolation functions are particularly important.

2. Governing equations

The energy transfer in DC casting can be reasonably represented in the framework of the one-phase continuum formulation (Bennon and Incropera, 1987) with the classical solid-liquid constitutive relations. Consider a connected fixed domain Ω with boundary Γ occupied by a phase change material described with the temperature dependent density $\varrho_{\mathcal{P}}$, specific heat at constant pressure $c_{p\mathcal{P}}$ and the thermal conductivity $k_{\mathcal{P}}$ of the solid $\mathcal{P} = \mathcal{S}$ and the liquid $\mathcal{P} = \mathcal{L}$ phase, and the specific latent heat of the solid-liquid phase change $h_{\mathcal{M}}$. The one-phase continuum formulation of the energy transport for the assumed system is

$$\frac{\partial}{\partial t}(f_{\mathcal{S}}\,\varrho_{\mathcal{S}}\,h_{\mathcal{S}} + f_{\mathcal{L}}\,\varrho_{\mathcal{L}}\,h_{\mathcal{L}}) + \nabla\cdot(f_{\mathcal{S}}\,\varrho_{\mathcal{S}}\,h_{\mathcal{S}}\,\mathbf{v}_{\mathcal{S}} + f_{\mathcal{L}}\,\varrho_{\mathcal{L}}\,h_{\mathcal{L}}\,\mathbf{v}_{\mathcal{L}}) = -\nabla\cdot(f_{\mathcal{S}}\,\mathbf{F}_{\mathcal{S}} + f_{\mathcal{L}}\,\mathbf{F}_{\mathcal{L}}). \tag{1}$$

Function $f_{\mathcal{P}}$ denotes the temperature dependent volume fraction, $h_{\mathcal{P}}$ the specific enthalpy, $\mathbf{v}_{\mathcal{P}}$ the known velocity, and $\mathbf{F}_{\mathcal{P}}$ the heat flux of phase $\mathcal{P}$. Since only two phases are present in the system, $f_{\mathcal{S}} + f_{\mathcal{L}} = 1$. Due to assumed local thermal equilibrium between the phases, the phase temperatures are equal and represented by T. The phase change takes place between solidus $T_{\mathcal{S}}$ and liquidus temperature $T_{\mathcal{L}}$. Mean phase change temperature $T_{\mathcal{M}}$ and phase change interval $T_{\mathcal{LS}}$ are $T_{\mathcal{M}} = \frac{1}{2}\, T_{\mathcal{S}} + \frac{1}{2}\, T_{\mathcal{L}}$, $T_{\mathcal{LS}} = T_{\mathcal{L}} - T_{\mathcal{S}}$. Pure substances are modelled by a narrow phase change interval with $T_{\mathcal{M}}$ in this case standing for melting temperature. Constitutive relations for the heat fluxes are based on the Fourier relation $\mathbf{F}_{\mathcal{P}} = -\, k_{\mathcal{P}}\, \nabla T$, and the two enthalpy-temperature relationships with neglected pressure influence are

$$h_{\mathcal{S}} = \int_{T_h}^{T} c_{p\mathcal{S}}(\theta)\, d\theta, \quad h_{\mathcal{L}} = h_{\mathcal{S}}(T_{\mathcal{S}}) + \int_{T_{\mathcal{S}}}^{T} c_{p\mathcal{L}}(\theta)\, d\theta + h_{\mathcal{M}}, \tag{2}$$

with T_h representing the enthalpy reference temperature. The governing equation could be rewritten in the following latent heat source term form

$$\varrho_0\, c\, \frac{\partial T}{\partial t} + \nabla \cdot \mathbf{\Phi} = \nabla \cdot (\, k\, \nabla T\,) - \varrho_0\, h_{\mathcal{LS}}\, \frac{df_{\mathcal{L}}}{dt} \tag{3}$$

Specific heat c and thermal conductivity k of the continuum are defined as

$$\varrho_0\, c = f_{\mathcal{S}}\, h_{\mathcal{S}}\, \frac{d\varrho_{\mathcal{S}}}{dT} + f_{\mathcal{L}}\, h_{\mathcal{L}}\, \frac{d\varrho_{\mathcal{L}}}{dT} + f_{\mathcal{S}}\, \varrho_{\mathcal{S}}\, c_{p\mathcal{S}} + f_{\mathcal{L}}\, \varrho_{\mathcal{L}}\, c_{p\mathcal{L}} \tag{4}$$

$$k = f_{\mathcal{S}}\, k_{\mathcal{S}} + f_{\mathcal{L}}\, k_{\mathcal{L}} \tag{5}$$

with the representative density ϱ_0 of the system

$$\varrho_0 = \frac{1}{2}\, \varrho_{\mathcal{S}}(T_{\mathcal{M}}) + \frac{1}{2}\, \varrho_{\mathcal{L}}(T_{\mathcal{M}}) \tag{6}$$

and the enthalpy difference $h_{\mathcal{LS}}$

$$\varrho_0\, h_{\mathcal{LS}} = \varrho_{\mathcal{L}}\, h_{\mathcal{L}} - \varrho_{\mathcal{S}}\, h_{\mathcal{S}} \tag{7}$$

The abbreviation in the convection term is

$$\mathbf{\Phi} = f_{\mathcal{S}}\, \varrho_{\mathcal{S}}\, h_{\mathcal{S}}\, \mathbf{v}_{\mathcal{S}} + f_{\mathcal{L}}\, \varrho_{\mathcal{L}}\, h_{\mathcal{L}}\, \mathbf{v}_{\mathcal{L}} \tag{8}$$

We seek the solution of the governing equation for the thermal field at final time $t = t_0 + \Delta t$, where t_0 represents initial time and Δt the positive increment of the coordinate z. The solution is constructed by the initial and boundary conditions that follow. The initial temperature $T(\mathbf{p}, t_0)$ at point with position vector $\mathbf{p}$ and time t_0 is defined through the known function T_0;

$$T(\mathbf{p}, t_0) = T_0;\ \mathbf{p} \in \Omega \cup \Gamma \tag{9}$$

The boundary Γ is divided into not necessarily connected parts Γ^D, Γ^N, and Γ^R;

$$\Gamma = \Gamma^D \cup \Gamma^N \cup \Gamma^R, \tag{10}$$

with Dirichlet, Neumann, and Robin type boundary conditions respectively. These boundary conditions are at point $\mathbf{p}$ and time $t_0 \leq t \leq t_0 + \Delta t$ defined through known functions T_Γ, F_Γ, and $\mathcal{H}_\Gamma$:

$$T(\mathbf{p}, t) = T_\Gamma;\ \mathbf{p} \in \Gamma^D \tag{11}$$

$$\frac{\partial T}{\partial n_\Gamma}(\mathbf{p}, t) = -\frac{F_\Gamma}{k};\ \mathbf{p} \in \Gamma^N \tag{12}$$

$$\frac{\partial T}{\partial n_\Gamma}(\mathbf{p}, t) = -\frac{\mathcal{H}_\Gamma}{k}\,(\,T - T_{\Gamma\,\mathrm{ref}}\,);\ \mathbf{p} \in \Gamma^R \tag{13}$$

where the heat transfer coefficient $\mathcal{H}_\Gamma$ and other known functions are allowed to depend arbitrarily on the thermal field. The outward pointing normal on Γ is denoted by $\mathbf{n}_\Gamma(\mathbf{p})$. The considered physical model for energy transfer is already fully compatible with the momentum transfer and could be easily upgraded with the influence of the species transfer.

Equation (3) is rewritten by introducing the Kirchhoff variable

$$\mathcal{T}(T) = T_\mathcal{T} + \int_{T_\mathcal{T}}^{T} \frac{k(\theta)}{k_0}\, d\theta, \tag{14}$$

defined with representative thermal conductivity $k_0 = \frac{1}{2}\, k_\mathcal{S}(T_\mathcal{M}) + \frac{1}{2}\, k_\mathcal{L}(T_\mathcal{M})$, and with the Kirchhoff variable reference temperature $T_\mathcal{T}$. Knowledge of the inverse Kirchhoff function $T = T(\mathcal{T})$ is assumed as well. The governing equation is accordingly reformulated as

$$\varrho_0\, k_0\, \frac{c}{k}\, \frac{\partial}{\partial t}\mathcal{T} + \nabla \cdot \mathbf{\Phi} = k_0\, \nabla^2 \mathcal{T} - \varrho_0\, h_{\mathcal{LS}}\, \frac{\partial}{\partial t} f_\mathcal{L}, \tag{15}$$

the initial conditions as

$$\mathcal{T}(\mathbf{p}, t_0) = \mathcal{T}(T_0);\ \mathbf{p} \in \Omega \tag{16}$$

and the boundary conditions as

$$\mathcal{T}(\mathbf{p}, t) = \mathcal{T}(T_\Gamma);\ \mathbf{p} \in \Gamma^D \tag{17}$$

$$\frac{\partial \mathcal{T}}{\partial n_\Gamma}(\mathbf{p}, t) = -\frac{F_\Gamma}{k_0};\ \mathbf{p} \in \Gamma^N \tag{18}$$

$$\frac{\partial \mathcal{T}}{\partial n_\Gamma}(\mathbf{p},t) = -\frac{\mathcal{H}_\Gamma}{k_0}\,(\,T(\mathcal{T}) - T_{\Gamma\,\mathrm{ref}}\,);\ \mathbf{p} \in \Gamma^R. \tag{19}$$

The transformed equation (15) with transformed initial and boundary conditions is solved for $\frac{\partial \mathcal{T}}{\partial n_\Gamma}(\mathbf{p}, t_0 + \Delta t);\ \mathbf{p} \in \Gamma^D$, $\mathcal{T}(\mathbf{p}, t_0 + \Delta t);\ \mathbf{p} \in \Omega \cup \Gamma^N \cup \Gamma^R$, giving the required thermal field through the inverse Kirchhoff function.

The reformulation of the expressions associated with equation (3) into expressions associated with equation (15) is required in order to linearize the diffusion term. This enables its representation as a boundary integral after weighting with the fundamental solution of the Laplace equation.

3. Numerical method

The numerical method is presented in three logical entities: time discretization, iteration over timestep, and space discretization, as follows.

3.1 Time discretization

Time discretization of equation (15) is performed with the simple two-level finite differencing

$$\varrho_0\, k_0\, (\frac{c}{k})^{j+\iota}\, \frac{1}{\Delta t}\,(\,\mathcal{T}^{j+1} - \mathcal{T}^{j}\,) + \iota\,\nabla\cdot\mathbf{\Phi}^{j+1} + (1-\iota)\,\nabla\cdot\mathbf{\Phi}^{j}$$

$$= k_0\,(\iota\,\nabla^2\mathcal{T}^{j+1} + (1-\iota)\,\nabla^2\mathcal{T}^{j}) - \varrho_0\, h_{\mathcal{LS}}^{j+\iota}\,\frac{1}{\Delta t}(f_{\mathcal{L}}^{j+1} - f_{\mathcal{L}}^{j}) \tag{20}$$

where indexes j and j+1 represent values at t_0 and $t_0 + \Delta t$. Coefficient $\iota = 1$ gives fully implicit, and $\iota = 1/2$ Crank-Nicolson scheme.

3.2 Iteration over timestep

Since material properties, liquid volume fraction, convection term and boundary conditions in general depend on temperature, iterations over the timestep are inherently required in order to find the solution. The arbitrary temperature-dependent quantity ϖ at iteration level m+1 and time level $j + \iota$ is calculated as

$${}^{1}\varpi^{j+\iota} = \varpi^{j},$$

$${}^{m+1}\varpi^{j+\iota} = \iota\,{}^{m+1}\varpi^{j+1} + (1-\iota)\,\varpi^{j};\, m \geq 1 \tag{21}$$

with

$${}^{m+1}\varpi^{j+1} = \varpi(T({}^{m}\mathcal{T}^{j+1})) + c_\varpi\,[\,\varpi(T({}^{m+1}\mathcal{T}^{j+1})) - \varpi(T({}^{m}\mathcal{T}^{j+1})\,] \tag{22}$$

and c_ϖ representing the material property under-relaxation factor. The calculation $\varpi(T(\mathcal{T}))$ is required because the material properties as well as

possible correlations hidden in $\mathcal{H}$ are standardly given in terms of temperature instead of the Kirchhoff variable.

The liquid volume fraction at iteration level m+1 is approximated with the Kirchhoff variable at iteration level m+1 (Voller-Swaminathan (1991) ansatz)

$$ {}^{1}f_{\mathcal{L}}^{j+1} = f_{\mathcal{L}}^{j} $$

$$ {}^{m+1}f_{\mathcal{L}}^{j+1} = {}^{m}f_{\mathcal{L}}^{j+1} + {}^{m}\left(\frac{k_0}{k}\frac{df_{\mathcal{L}}}{dT}\right)^{j+1}\left({}^{m+1}\mathcal{T}^{j+1} - \mathcal{T}({}^{m}f_{\mathcal{L}}^{j+1})\right); m \geq 1 \tag{23} $$

The convection term at iteration level m+1 is expanded similarly as

$$ {}^{1}\mathbf{\Phi}^{j+1} = \mathbf{\Phi}^{j} $$

$$ {}^{m+1}\mathbf{\Phi}^{j+1} = {}^{m}\mathbf{\Phi}^{j+1} + {}^{m}\left(\frac{k_0}{k}\frac{\partial\mathbf{\Phi}}{\partial f_{\mathcal{L}}}\frac{df_{\mathcal{L}}}{dT}\right)^{j+1}\left({}^{m+1}\mathcal{T}^{j+1} - \mathcal{T}({}^{m}f_{\mathcal{L}}^{j+1})\right)+ $$

$$ {}^{m}\left(\frac{k_0}{k}\left(\frac{\partial\mathbf{\Phi}}{\partial\varrho_{\mathcal{S}}}\frac{d\varrho_{\mathcal{S}}}{dT} + \frac{\partial\mathbf{\Phi}}{\partial\varrho_{\mathcal{L}}}\frac{d\varrho_{\mathcal{L}}}{dT} + \frac{\partial\mathbf{\Phi}}{\partial h_{\mathcal{S}}}\frac{dh_{\mathcal{S}}}{dT} + \frac{\partial\mathbf{\Phi}}{\partial h_{\mathcal{L}}}\frac{dh_{\mathcal{L}}}{dT}\right)\right)^{j+1} \left({}^{m+1}\mathcal{T}^{j+1} - {}^{m}\mathcal{T}^{j+1}\right); m \geq 1 \tag{24} $$

with the explicit form of derivatives

$$ \frac{\partial\mathbf{\Phi}}{\partial f_{\mathcal{L}}}\frac{df_{\mathcal{L}}}{dT} = \left(\varrho_{\mathcal{L}}\, h_{\mathcal{L}}\, \mathbf{v}_{\mathcal{L}} - \varrho_{\mathcal{S}}\, h_{\mathcal{S}}\, \mathbf{v}_{\mathcal{S}}\right)\frac{df_{\mathcal{L}}}{dT}, $$

$$ \frac{\partial\mathbf{\Phi}}{\partial\varrho_{\mathcal{P}}}\frac{d\varrho_{\mathcal{P}}}{dT} = f_{\mathcal{P}}\, h_{\mathcal{P}}\, \mathbf{v}_{\mathcal{P}}\, \frac{d\varrho_{\mathcal{P}}}{dT}, $$

$$ \frac{\partial\mathbf{\Phi}}{\partial h_{\mathcal{P}}}\frac{dh_{\mathcal{P}}}{dT} = f_{\mathcal{P}}\, \varrho_{\mathcal{P}}\, \mathbf{v}_{\mathcal{P}}\, c_{p\mathcal{P}} \tag{25} $$

Function $\mathcal{T}(f_{\mathcal{L}})$ is defined as

$$ \mathcal{T}(f_{\mathcal{L}}) = \begin{cases} \mathcal{T}(T_{\mathcal{S}}); & f_{\mathcal{L}} = 0 \\ \mathcal{T}(T(f_{\mathcal{L}})); & 0 < f_{\mathcal{L}} < 1 \\ \mathcal{T}(T_{\mathcal{L}}); & f_{\mathcal{L}} = 1 \end{cases} \tag{26} $$

The adjacent iterative treatment of boundary conditions is

$$ {}^{m+1}\mathcal{T}^{j+\iota} = \iota\,\mathcal{T}({}^{m}T_{\Gamma}^{j+1}) + (1-\iota)\,\mathcal{T}(T_{\Gamma}^{j}); \quad \mathbf{p} \in \Gamma^{D}, \tag{27} $$

$$ {}^{m+1}\frac{\partial \mathcal{T}^{j+\iota}}{\partial n_\Gamma} = -\iota\,\frac{{}^{m}F_\Gamma{}^{j+1}}{k_0} - (1-\iota)\,\frac{F_\Gamma{}^{j}}{k_0}; \quad \mathbf{p} \in \Gamma^N, \tag{28} $$

$$ {}^{m+1}\frac{\partial \mathcal{T}^{j+\iota}}{\partial n_\Gamma} = -\iota\left[\frac{{}^{m}\mathcal{H}_\Gamma}{{}^{m}k}\,{}^{m+1}\mathcal{T} - \frac{{}^{m}\mathcal{H}_\Gamma}{k_0}\left({}^{m}T_{\Gamma\,\mathrm{ref}} - {}^{m}T + \frac{k_0}{{}^{m}k}\,{}^{m}\mathcal{T}\right)\right]^{j+1} $$

$$ -(1-\iota)\left[\frac{\mathcal{H}_\Gamma}{k_0}\left(T - T_{\Gamma\,\mathrm{ref}}\right)\right]^{j}; \quad \mathbf{p} \in \Gamma^R. \tag{29} $$

The Robin boundary conditions (29) have been split into a form which permits calculation of the unknown ${}^{m+1}\mathcal{T}^{j+1}$.

The final time-discretized form of equation (15) is obtained by inserting the $m+1$ iteration level material properties, liquid volume fraction, and convection term expansions into equation (20).

3.3 Iterative updating

After discretization over space and calculation of the Kirchhoff variable field (and subsequently the temperature field) at time $j+1$ and iteration $m+1$, elaborated in the next chapter, the quantities involved have to be updated for the next iteration. The temperature dependent quantities are updated from (21), the convection term is updated from equation (24) and the boundary conditions are updated from equations (27-29). Two different situations can occur regarding the liquid volume fraction updating, the first one with the liquid volume fraction at time $j+1$ and iteration level m in the phase change interval $0 < {}^{m}f_{\mathcal{L}}^{j+1} < 1$, and the second one outside the phase-change interval ${}^{m}f_{\mathcal{L}}^{j+1} = 0$ or ${}^{m}f_{\mathcal{L}}^{j+1} = 1$. In the first case, the liquid volume fraction is updated directly from equation (23). In the second case, the derivative $df_{\mathcal{L}}/dT$ equals zero and the melting or solidification process (transition from outside the phase-change interval into the phase-change interval) can not be started when using the above-mentioned formula. A suitable updating strategy for such cases is

$$ {}^{m+1}f_{\mathcal{L}}^{j+1} = {}^{m}f_{\mathcal{L}}^{j+1} + {}^{m}\left(\frac{c}{h_{\mathcal{LS}}}\,\frac{k_0}{k}\right)^{j+\iota}\left({}^{m+1}\mathcal{T}^{j+1} - \mathcal{T}({}^{m}f_{\mathcal{L}}^{j+1})\right) \tag{30} $$

A derivation of formula (30) which is similar to the first one with $df_{\mathcal{L}}/dT$ replaced by $c/h_{\mathcal{LS}}$ can be found in Šarler and Kuhn (1998a). Since both updating formulas (23,30) could give physically impossible liquid volume fractions (less than 0 or greater than 1), updating is corrected by the over/under-shoot formula

$$ {}^{m+1}f_{\mathcal{L}}^{j+1} = \begin{cases} 1; & {}^{m+1}f_{\mathcal{L}}^{j+1} > 1 \\ {}^{m+1}f_{\mathcal{L}}^{j+1}; & 0 < {}^{m+1}f_{\mathcal{L}}^{j+1} < 1 \\ 0; & {}^{m+1}f_{\mathcal{L}}^{j+1} < 0 \end{cases} \tag{31} $$

The internal timestep iterations are stopped when the maximum absolute value of the one-phase enthalpy $h = (\rho_S/\rho_0) f_S h_S + (\rho_L/\rho_0) f_L h_L$ difference between two successive iterations does not exceed some predetermined small positive h_{err}

$$\max |^{m+1}h^{j+1} -^{m} h^{j+1}| < h_{\text{err}} \tag{32}$$

The discussed updating is in principle based on the Voller-Swaminathan idea (Voller and Swaminathan, 1991), however it has been extended in the present context to the convection term and put into Kirchhoff variable perspective. The principal difference originates in the second updating formula (30) which is in our work independent of space discretization. Therefore, from this point of the derivation onward one can continue with any space discretization procedure.

3.4 Space discretization

The DRBEM space discretization is applied in the present work. Respectively, space discretization is made by weighting the time-discretized equation (15) over domain Ω with the fundamental solution of the Laplace equation $T^*(\mathbf{p};\mathbf{s})$. $\mathbf{p}$ stands for the field point and $\mathbf{s}$ for the source point position vector. The integral type ($\mathcal{F}$ denotes the arbitrary scalar and $\mathcal{G}$ the arbitrary vector valued function respectively)

$$\mathcal{I}_1 = \int_\Omega \mathcal{F}(\mathbf{p})\, T^*(\mathbf{p};\mathbf{s})\, d\Omega \tag{33}$$

arises when weighting the transience and source terms,

$$\mathcal{I}_2 = \int_\Omega \nabla \cdot \mathcal{G}(\mathbf{p})\, T^*(\mathbf{p};\mathbf{s})\, d\Omega \tag{34}$$

when weighting the convection term, and

$$\mathcal{I}_3 = \int_\Omega \nabla^2 \mathcal{F}(\mathbf{p})\, T^*(\mathbf{p};\mathbf{s})\, d\Omega \tag{35}$$

when weighting the diffusion term. Let us focus on axisymmetric (coordinates r, z of the field point and coordinates r_s, z_s of the source point) geometry and field situations, e.g.

$$T^*(\mathbf{p};\mathbf{s}) = \frac{1}{\pi \rho}\, \mathrm{K}(\tilde{\rho}), \tag{36}$$

with $\rho^2 = (r + r_s)^2 + (z - z_s)^2$, $\tilde{\rho} = 2 r r_s/\rho$, and K standing for a complete elliptic integral of the first kind. Boundary geometry is approximated by N_Γ straight line segments, and spatial variation of the fields on each of the boundary segments is represented by constant interpolation functions with meshpoints coinciding with the geometrical centres of the straight line segments. Spatial variation of the fields in Ω is represented by the N_ψ global

interpolation functions (Partidge *et al.*, 1992) of the form (Einstein summation convention is used in this text, i.e. any index that is repeated twice in a product is summed on, underlined index is not summed on)

$$\mathcal{F}(\mathbf{p}) \approx \psi_u(\mathbf{p})\, \varsigma_u, \tag{37}$$

collocating $N = N_\Gamma + N_\Omega$ meshpoints $\mathbf{p}_n$ with coordinates r_n, z_n. (the first N_Γ collocation points coincide with the boundary meshpoints and the remaining N_Ω are arbitrarily distributed in the domain). Coefficients ς_u are calculated by constructing (Powell, 1993) a system of N_ψ algebraic equations

$$\boldsymbol{\Psi}\, \boldsymbol{\varsigma} = \boldsymbol{\mathcal{F}} \tag{38}$$

The vectors are $\boldsymbol{\varsigma} = (\varsigma_1, \varsigma_2, \cdots, \varsigma_{N_\psi})^{\mathrm{t}}$ and $\boldsymbol{\mathcal{F}} = (\mathcal{F}_1, \mathcal{F}_2, \cdots, \mathcal{F}_N, 0, \cdots, 0)^{\mathrm{t}}$. The first N rows of matrix $\boldsymbol{\Psi}$ are of the form $(\psi_{v1}, \psi_{v2}, \cdots, \psi_{vN_\psi})$, and the remaining rows are of the form $(\psi_{1v}, \psi_{2v}, \cdots, \psi_{Nv}, 0, \cdots, 0)$, where the notation has been shortened to $\mathcal{F}_n \equiv \mathcal{F}(\mathbf{p}_n)$, $\psi_{nu} \equiv \psi_u(\mathbf{p}_n)$. Coefficients ς_u follow by inverting the system of algebraic equations

$$\boldsymbol{\varsigma} = \boldsymbol{\Psi}^{-1}\, \boldsymbol{\mathcal{F}} \tag{39}$$

Selection of simply augmented thin plate splines (Golberg and Chen, 1994) for ψ_u gives an optimal approximating property. The axisymmetric form of these functions has been found to be (the details of the relatively lengthy derivation can be found in Šarler (1998))

$$\psi_n = 4\, \rho_n\, \mathrm{E}(\tilde{\rho}_n); \quad {}_{n=1,2,\cdots,N},$$

$$\psi_{N+1} = 1,$$

$$\psi_{N+2} = (z - z_0) \tag{40}$$

with $\rho_n^2 = (r + r_n)^2 + (z - z_n)^2$, $\tilde{\rho}_n = 2\, r\, r_n / \rho_n$, and E standing for a complete elliptic integral of the second kind. If the symmetry axis does not cross Ω, additional augmentation with

$$\psi_{N+3} = \log r - \log r_0 \tag{41}$$

is appropriate. Constants r_0 and z_0 represent mean coordinates of the domain Ω. The scaling constant z_0 assures the translatory symmetry of the computations in the direction of the symmetry axis.

The integral type $\mathcal{I}_3$ is calculated by using Green's second identity

$$\mathcal{I}_{3l} \approx G_{lk}\, \delta_{ki}\, \frac{\partial \mathcal{F}_i}{\partial n_\Gamma} - H_{lk}\, \delta_{ki}\, \mathcal{F}_i - \underline{c_l^*}\, \delta_{li}\, \mathcal{F}_i;$$

$$G_{lk} = \int_{\Gamma_k} T_l^* \, r \, dr \, dz, \quad H_{lk} = \int_{\Gamma_k} \frac{\partial T_l^*}{\partial n_\Gamma} \, r \, dr \, dz, \tag{42}$$

where $k = 1, 2, \cdots N_\Gamma$ and $i, l = 1, 2, \cdots N$. Index l stands for $\mathbf{s}_l = \mathbf{p}_l$, Γ_k represents the k-th boundary segment in generating axisymmetric plane, and c_l^* is equal to $c_l^* = \frac{1}{2}$; $\mathbf{s}_l \in \Gamma$, $c_l^* = 1$; $\mathbf{s}_l \in \Omega$. The integral types $\mathcal{I}_1$ and $\mathcal{I}_2$ are calculated by defining the harmonic functions $\nabla^2 \hat{\psi}_u(\mathbf{p}) = \psi_u(\mathbf{p})$. Consequently, integral types $\mathcal{I}_1$ and $\mathcal{I}_2$ could be written in a compact dual reciprocity form

$$\mathcal{I}_{1l} \approx \Psi_{lu} \, \Psi_{ui}^{-1} \, \mathcal{F}_i,$$

$$\mathcal{I}_{2l} \approx \left[\Psi_{ln} \, \Psi_{ni}^{-1} \, \frac{1}{p_{r\underline{i}}} + \Psi_{rln} \, \Psi_{ni}^{-1} \right] \mathcal{G}_{ir} + \Psi_{zln} \, \Psi_{ni}^{-1} \, \mathcal{G}_{iz}; \tag{43}$$

with

$$\Psi_{lu} \approx G_{lk} \, \delta_{ki} \, \frac{\partial \hat{\psi}_{iu}}{\partial n_\Gamma} - H_{lk} \, \delta_{ki} \, \hat{\psi}_{iu} - c_{\underline{l}}^* \, \delta_{li} \, \hat{\psi}_{iu},$$

$$\Psi_{\zeta lu} \approx G_{lk} \, \delta_{ki} \, \frac{\partial}{\partial n_\Gamma} \frac{\partial \hat{\psi}_{iu}}{\partial p_\zeta} - H_{lk} \, \delta_{ki} \, \frac{\partial \hat{\psi}_{iu}}{\partial p_\zeta} - c_{\underline{l}}^* \, \delta_{li} \, \frac{\partial \hat{\psi}_{iu}}{\partial p_\zeta} \tag{44}$$

Index ζ could take values r, z, and indexes o, u, and v run over $o = 1, 2, \cdots, N$, $u, v = 1, 2, \cdots, N_\psi$. The formulation of the convection term used in this paper is much more efficient and accurate than the forms used previously (Wrobel and DeFigueredo, 1991) in the context of the variable velocity fields, since they originate from the conservation form of the convection term instead of other derived forms. Axisymmetric functions $\hat{\psi}_n$ have been found to be

$$\hat{\psi}_n = \frac{1}{18\,\pi} \rho_n^3 \, [2\,(2 - \tilde{\rho}_n^2)\,\mathrm{E}(\tilde{\rho}_n) - (1 - \tilde{\rho}_n^2)\,\mathrm{K}(\tilde{\rho}_n)\,]; \quad {\scriptstyle n=1,2,\cdots,N},$$

$$\hat{\psi}_{N+1} = \frac{1}{6} \, [\, r^2 - {r_0}^2 + (z - z_0)^2 \,],$$

$$\hat{\psi}_{N+2} = \frac{1}{6} \, (z - z_0)^3,$$

$$\hat{\psi}_{N+3} = \frac{1}{6} \, r^2 \, (\log r - \log r_0). \tag{45}$$

After weighting the time discretized governing equation with the fundamental solution of the Laplace equation and calculating the boundary and domain

integrals as described, the completely discretized form is structured. Rearrangement of its terms with respect to the boundary conditions gives a system of N algebraic equations for solving the unknowns ${}^{m+1}\mathcal{T}_n^{j+1}$ or ${}^{m}\frac{\partial \mathcal{T}^{j+1}}{\partial n_{\Gamma n}}$ on the boundary, and ${}^{m+1}\mathcal{T}_n^{j+1}$ in the domain. The explicit forms of the algebraic system of equations matrix elements are listed in (Šarler, Kuhn, 1998a) and the extensive testing of the present method for simple transient and steady-state situations can be found in Šarler and Kuhn (1998b).

4. DC casting model

The numerical examples in this paper are divided into two parts. In the first part, a comparison of the present method with the results of the classical finite volume method is given, based on a simplified model of the DC casting process. In the second part, the present method is used in a full-scale industrial process model that gives technologically relevant results. Let us first discuss common features used in both parts.

Only steady state solutions are shown in this paper. They have been approached by transient calculation using fixed timestep 5 [s] and fully implicit scheme. The criterion for reaching the steady-state is defined as

$$\max \mid \mathrm{h}^{\mathrm{j}+1} - \mathrm{h}^{\mathrm{j}} \mid < \mathrm{h}_{\mathrm{steady}} \tag{46}$$

The enthalpy iteration error h_{err} and the steady-state enthalpy criterion h_{steady} have been both set to $0.1\,[\mathrm{J}/(\mathrm{kg\,K})]$. The enthalpy T_h and the Kirchhoff reference temperature $T_{\mathcal{T}}$ have been both set to 0.0 [K].

The boundary element mesh for calculating the domain integrals of the global interpolation functions (see equation (44)) is made by uniform subdivision of the boundary elements into three sub-elements. The Kirchhoff transform and enthalpy are calculated analytically and the inverse Kirchhoff transform by the Van Wijngaarden-Dekker-Brent method (Press *et al.*, 1992) with an accuracy of 10^{-6}. The material properties under-relaxation factor was set to $c_{\varpi} = 1$.

System matrices are solved by the standard Gaussian elimination with rows and columns pivoting. The computer program has been coded in Fortran with double precision accuracy. Test cases have been run on a HP 9000 Series 700 Model 715/100 workstation. The regular integrals are calculated by the 8-point Gaussian quadrature, the weakly singular integrals (diagonal elements in matrix **G**) analytically, and the strongly singular integrals (diagonal elements in matrix **H**) by the thermal equilibrium technique. System matrices are solved by the standard Gaussian elimination with rows and columns pivoting.

4.1 Comparison with the FVM

The following simplified axisymmetric DC casting-like test case was considered for test comparison with the FVM. The computational domain is a solid cylinder $0.0\,[\mathrm{m}] \leq r \leq 0.25\,[\mathrm{m}]$, $0\,[\mathrm{m}] \leq z \leq -1.25\,[\mathrm{m}]$. The boundary conditions at the top of the cylinder at $z = 0\,[\mathrm{m}]$ are of the Dirichlet type with $T_{\Gamma} = 980\,[\mathrm{K}]$, and the boundary conditions at the bottom of the cylinder are of

the Neumann type with $F_\Gamma = 0\,[\mathrm{W/m^2}]$. The boundary conditions at the outer surface of the cylinder are of the Robin type with $T_{\Gamma\,\mathrm{ref}} = 298\,[\mathrm{K}]$. The heat transfer coefficient between $0\,[\mathrm{m}] \geq z > -0.01\,[\mathrm{m}]$, $-0.01\,[\mathrm{m}] \geq z > -0.06\,[\mathrm{m}]$, $-0.06\,[\mathrm{m}] \geq z > -0.10\,[\mathrm{m}]$, and $-0.10\,[\mathrm{m}] \geq z > -1.25\,[\mathrm{m}]$ are $\mathcal{H}_\Gamma = 0.0\,[\mathrm{W/(m^2\,K)}]$, $\mathcal{H}_\Gamma = 3000.0\,[\mathrm{W/(m^2\,K)}]$, $\mathcal{H}_\Gamma = 150.0\,[\mathrm{W/(m^2\,K)}]$, and $\mathcal{H}_\Gamma = 4000.0\,[\mathrm{W/(m^2\,K)}]$ respectively.

Material properties correspond to a simplified Al4.5 per cent Cu alloy and have been combined from Reddy and Beckermann (1997) and Pehlke *et al.* (1982): $\rho_\mathcal{S} = \rho_\mathcal{L} = 2982\,[\mathrm{kg/m^3}]$, $k_\mathcal{S} = 120.7\,[\mathrm{W/m\,K}]$, $k_\mathcal{L} = 57.3\,[\mathrm{W/m\,K}]$, $c_\mathcal{S} = 1032.0\,[\mathrm{W/m\,K}]$, $c_\mathcal{L} = 1179.0\,[\mathrm{W/m\,K}]$, $h_\mathcal{M} = 3482000.0\,[\mathrm{J/kg\,K}]$, $T_\mathcal{S} = 775.0\,[\mathrm{K}]$, $T_\mathcal{L} = 911.0\,[\mathrm{K}]$. The liquid fraction increases linearly between $T_\mathcal{S}$ and $T_\mathcal{L}$. The initial conditions grow linearly with the z coordinate from 298 [K] at the bottom to 980 [K] at the top of the cylinder. The uniform casting velocity is $v_{\mathcal{S}r} = v_{\mathcal{L}r} = 0\,[\mathrm{m/s}], v_{\mathcal{S}z} = v_{\mathcal{L}z} = -0.00633\,[\mathrm{m/s}]$.

Since the analytical solution to the posed problem is not known, classical FVM is used to obtain the reference solution for comparison. The FVM discretization technique is well-known and described in Patankar (1980). Axial symmetry is considered in the present case. Due to the low Péclet number the central difference scheme was used. Standard total enthalpy formulation of the energy conservation equation was used as for example in Bennon and Incropera (1988). The set of linear discretized equations resulting from the fully implicit time marching scheme for solving the energy conservation equation was solved with an ADI-like procedure using the Thomas algorithm for solving tridiagonal systems. A detailed description of the implementation can be found in Mencinger (1998).

The reference solution was obtained on a 25×125 uniform grid (see Figure 2) with 3,125 finite volumes and 50×250 uniform grid with 12,500 finite volumes. The CPU time required to run the cases was 1,264 and 8,121 seconds respectively. The comparison of both solutions in terms of the centerline temperature, middle radius temperature at $r = 0.25\,[\mathrm{m}]$ and boundary

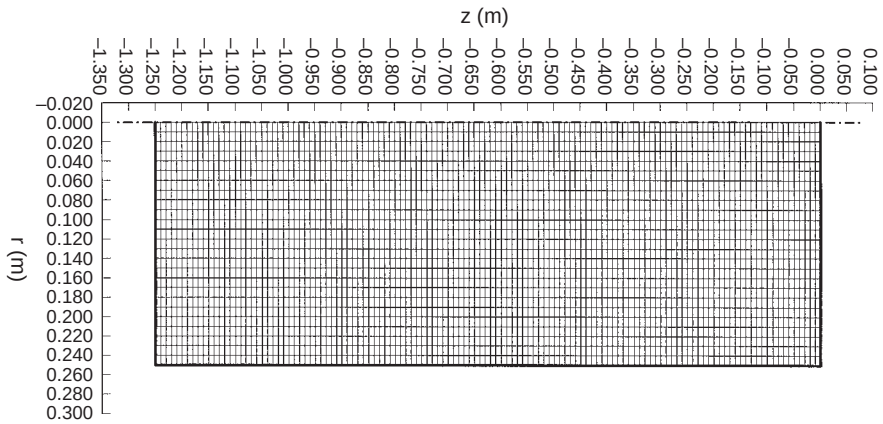

Figure 2.
Schematics of the FVM mesh 25×125 used in computations. The borders between the 3,125 finite volumes are shown. The related meshpoints (not plotted) are placed at the centres of the finite volumes

temperature is shown in Figure 4. The absolute difference of both FVM solutions at the mentioned three axial positions is shown in Figure 5. The maximum absolute error calculated in 126 uniform axial locations is 5.6 [K], 2.7 [K], and 6.3 [K] at the centerline, middle and surface, respectively. The scaling of the errors with the temperature difference of the process, i.e.

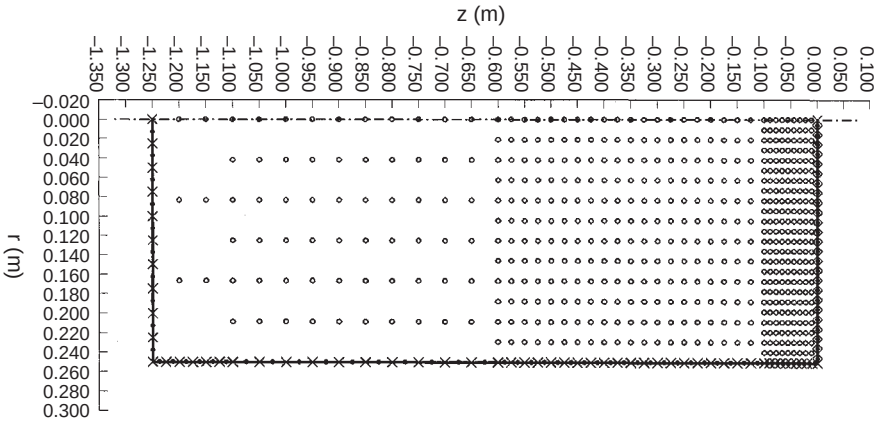

Figure 3.
Schematics of the DRBEM mesh used in computations. Boundary and domain meshpoints are denoted by • and ○ respectively. Boundary element borders are marked with ×

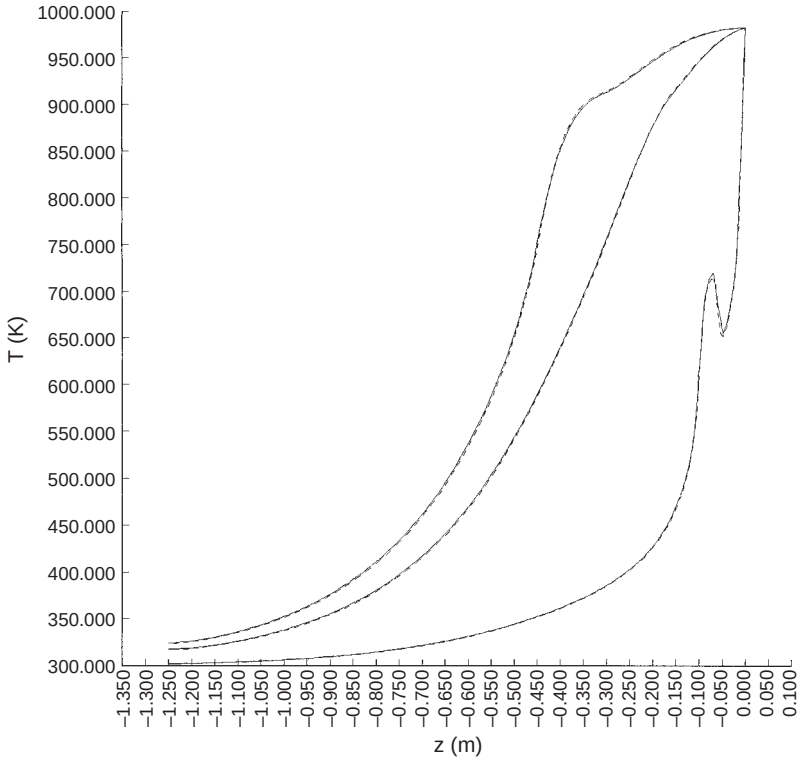

Figure 4.
First test case. The solid line denotes the temperatures calculated with the 25×125 FVM mesh and the dashed line the temperatures calculated with the 50×250 FVM mesh. Top curves – centreline, medium curves – mid-radius, and lower curves – surface temperature

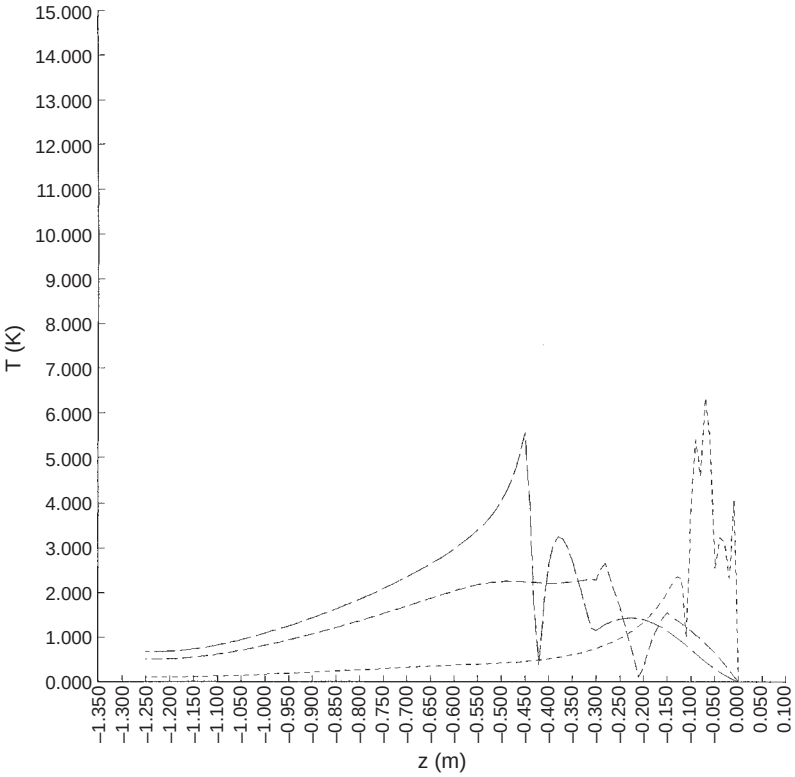

Figure 5.
First test case. Absolute difference between the two FVM solutions from Figure 4. Coarse dashed curve – centerline, medium dashed curve – mid-radius, and fine dashed curve – surface

290 [K] − 298 [K] gives a maximum relative error between the two meshes of less than 1 per cent and thus proves the reasonable mesh-independence of the FVM results.

The comparison of the DRBEM solution obtained with the non-uniform mesh from Figure 3 (with $N = 603, N_\Gamma = 81, N_\Omega = 522$) and the 50×250 FVM mesh at three radial locations is shown in Figure 6 and the maximum absolute error between the two solutions calculated at 126 uniform axial locations is shown in Figure 7. Related errors are 6.6 [K], 3.3 [K], and 14.6 [K] at the centerline, middle and surface, respectively. The scaling of the errors with the temperature difference of the process gives a maximum relative error between the two principally different discrete approximative solutions of less than 2.5 per cent. The maximum absolute errors between the two methods occur in the area of high surface gradients and are very localized as seen in Figure 7. Observation of the errors between both FVM results and results obtained by the fine-grid FVM method and DRBEM method proves the reasonable mesh-independence of the DRBEM results. This is somewhat surprising since the DRBEM solution is calculated on approximately 5 per cent of the gridpoints of the fine FVM mesh only and shows the high convergence rate of the DRBEM results. All figures calculated with DRBEM are generated from the

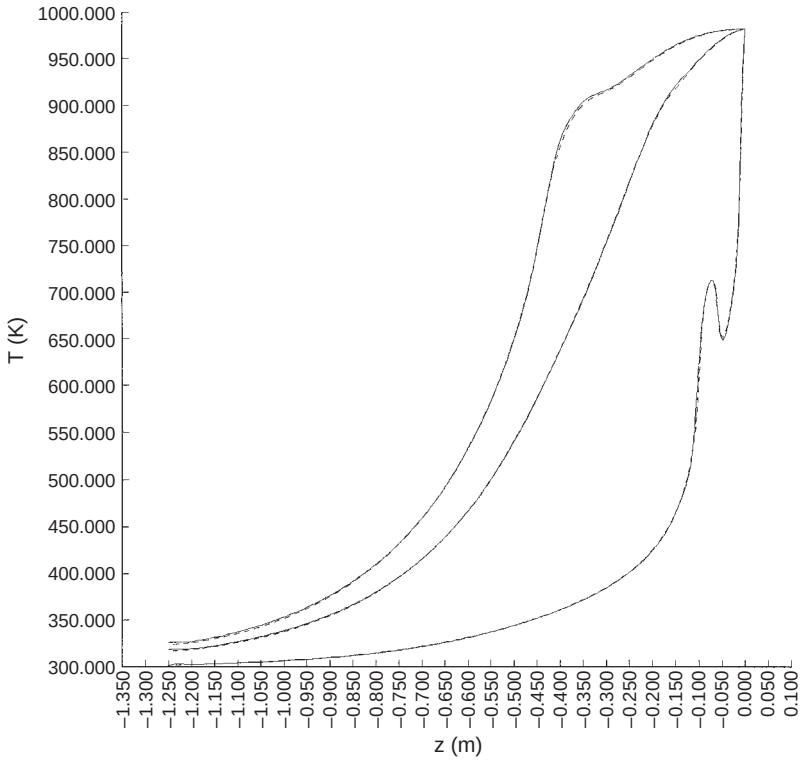

Figure 6.
First test case. The solid line denotes the temperatures calculated with the DRBEM mesh from Figure 2, and the dashed line the temperatures calculated with the 50×250 meshed FVM. Top curves – centerline, medium curves – mid-radius, and lower curves – surface temperature

axisymmetric augmented thin plate spline global interpolation as used in the calculations. The cylinder reaches steady-state in 246 timesteps with a maximum of six and an average number of 3.4 internal timestep iterations. Figure 8 presents the respective isotherms obtained with the DRBEM method. The CPU time for the test case is 2,880 seconds. Most of the computing time is spent on the solution of full asymmetric systems of algebraic equations.

4.2 DC casting model

The second example deals with the realistic model of the billet. The geometry of the billet, the space discretization, the boundary conditions at the top and at the bottom of the billet as well the initial conditions are assumed to be the same as in the first test case.

The boundary conditions at the outer surface of the billet are of the Robin type. They are divided into three regions. The first region $0.0\,[\mathrm{m}] \geq z > -0.095\,[\mathrm{m}]$ corresponds to the mould, the second region corresponds to the cooling gap $-0.950\,[\mathrm{m}] \geq z > -0.100\,[\mathrm{m}]$ (this is the gap between the lower end of the mould and the point at which water flowing from the mould impinges onto the surface of the billet), and the third region $-0.100\,[\mathrm{m}] \geq z \geq -1.250\,[\mathrm{m}]$ corresponds to the direct-chill region.

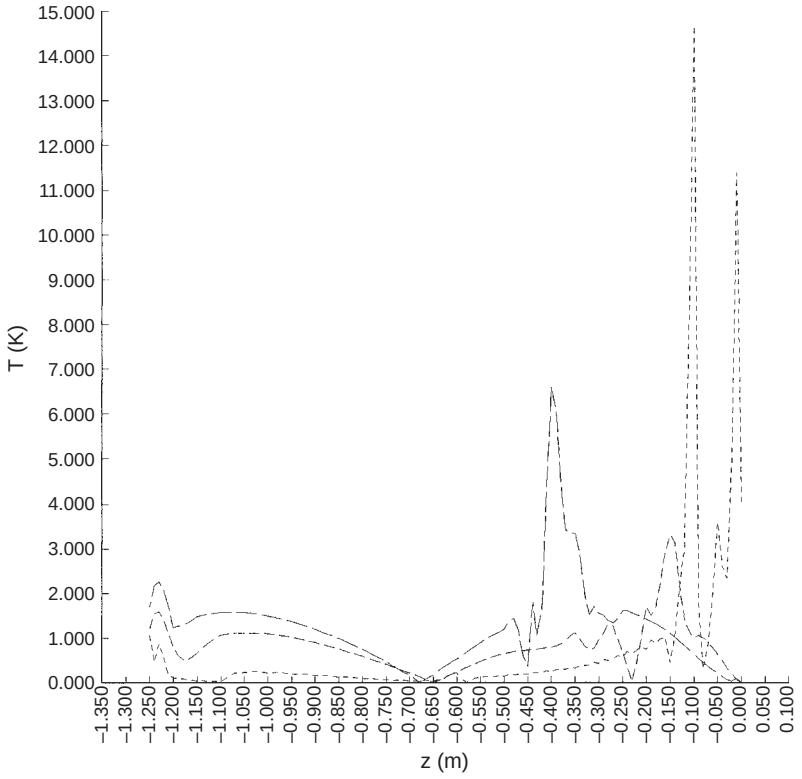

Figure 7.
First test case. Absolute difference between the FVM and the DRBEM solutions from Figure 6. Coarse dashed curve – centerline, medium dashed curve – mid-radius, and fine dashed curve – surface

The first centimeter at the top of the mould is assumed to be insulated. The heat transfer coefficient in the remaining part of the mould region (Katgerman *et al.*, 1990) is represented by the empirical correlation $\mathcal{H}_\Gamma[\mathrm{W}/(\mathrm{m}^2\,\mathrm{K})]$

$$\mathcal{H}_\Gamma = \mathcal{H}_{\Gamma\,\mathrm{high}}^{f_\mathcal{L}}\,\mathcal{H}_{\Gamma\,\mathrm{low}}^{1-f_\mathcal{L}} \tag{47}$$

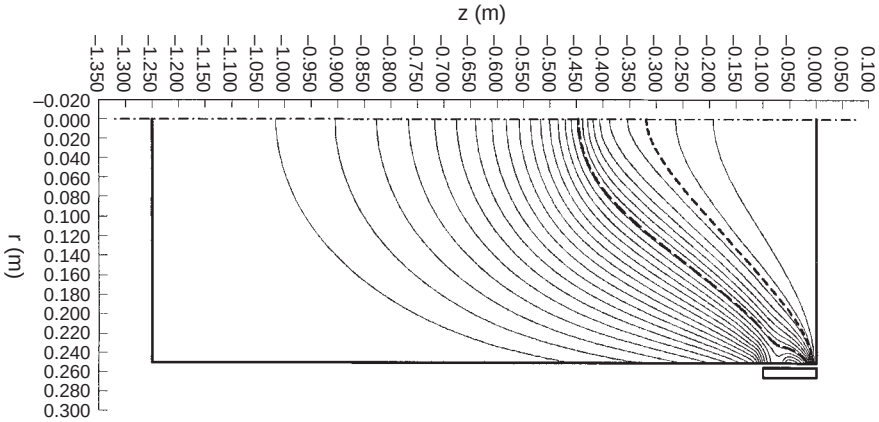

Figure 8.
First test case. DRBEM results. The bottom isotherm corresponds to 350[K]. The temperature difference between isotherms is 25[K]. Solidus and liquidus isotherms are bold and dashed

with $\mathcal{H}_{\Gamma\,\mathrm{high}} = 4000.0$ and $\mathcal{H}_{\Gamma\,\mathrm{low}} = 150.0$. This correlation takes into account the reduction of the heat transfer coefficient due to solidification shrinkage (formation of the air gap between billet outer surface and mould inner surface).

The heat transfer coefficient in the cooling gap region is represented by the constant heat transfer coefficient $\mathcal{H}_\Gamma = 150.0\,[\mathrm{W}/(\mathrm{m\,K})]$.

The heat transfer coefficient in the direct chill water cooled region is represented by the Weckman-Niessen (Weckman and Niessen, 1982) heat transfer correlation $\mathcal{H}_\Gamma\,[\mathrm{W}/(\mathrm{m\,K})]$

$$\mathcal{H}_\Gamma = (\,-1.67\,10^5 + 704.00\,\bar{T}_\Gamma\,)\,(\frac{Q}{2\,\pi\,r_{\max}})^{1/3} + \frac{20.80}{T_\Gamma - T_{\Gamma\,\mathrm{ref}}}\,(\,T_\Gamma - 373.15\,)^3 \tag{48}$$

where $T_\Gamma\,[\mathrm{K}]$ represents billet boundary temperature, $T_{\Gamma\,\mathrm{ref}}\,[\mathrm{K}]$ the bulk cooling water temperature, and $\bar{T}$ the mean temperature

$$\bar{T} = \frac{1}{2}\,(\,T_\Gamma + T_{\Gamma\,\mathrm{ref}}\,) \tag{49}$$

$Q[\mathrm{m}^3/\mathrm{s}]$ denotes the billet coolant flow and $r_{\max}\,[\mathrm{m}]$ the billet radius. The first

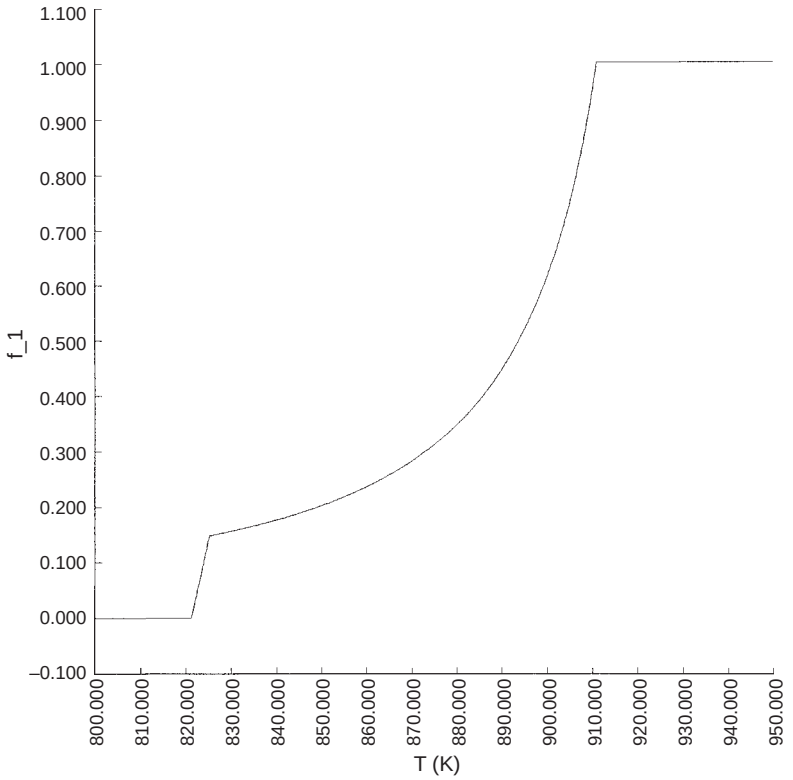

Figure 9.
The liquid fraction – temperature relationship from equation (51)

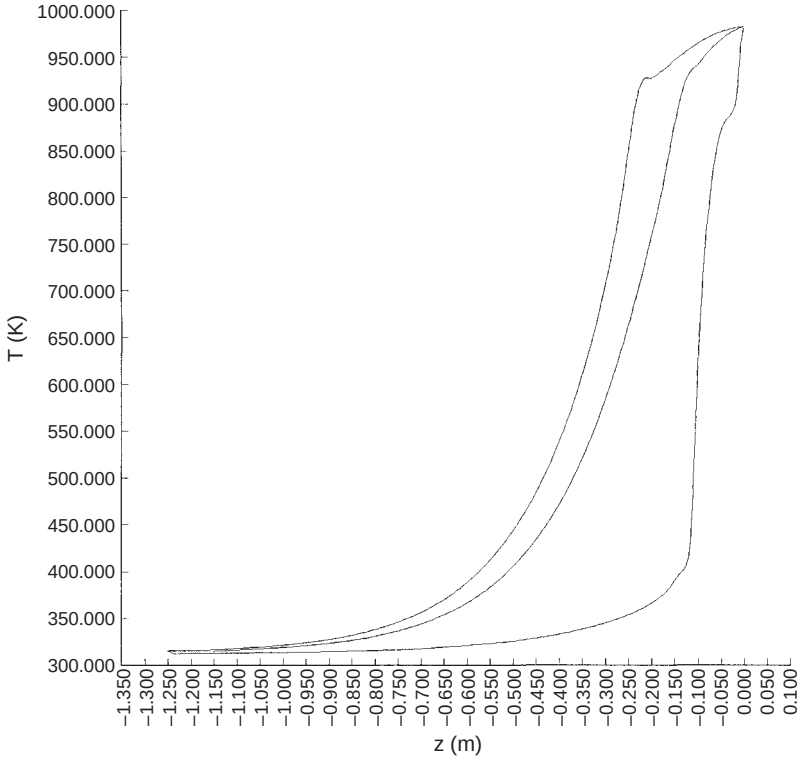

Figure 10.
Second test case. DRBEM results. Top curve – centerline, medium curve – mid-radius, and lower curve – surface temperature

term in correlation (48) accounts for convective heat transfer due to the one-phase free falling turbulent film of water, and the second term, which is taken into account only when $T_\Gamma > 373.15$ [K], models the subcooled nucleate boiling. The bulk water heating with the decreasing axial location is calculated as

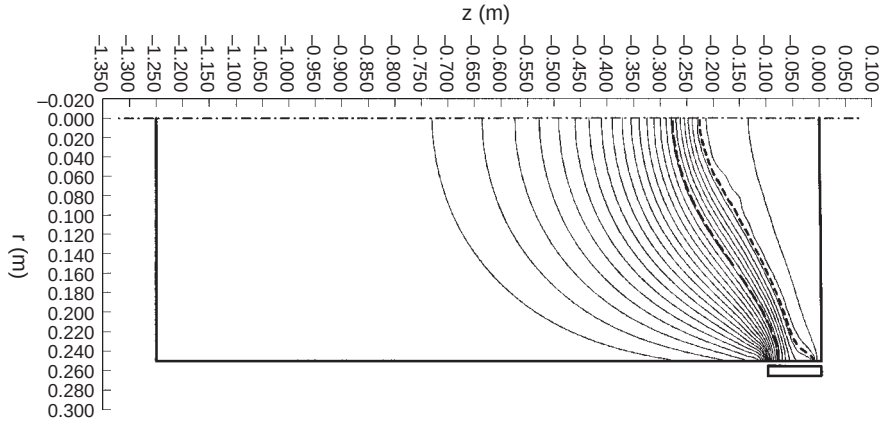

Figure 11.
Second test case. DRBEM results. The bottom isotherm corresponds to 350 [K]. The temperature difference between isotherms is 25 [K]. Solidus and liquidus isotherms are bold and dashed

$$T_{\Gamma\,\mathrm{ref}}(z-\Delta z) = T_{\Gamma\,\mathrm{ref}}(z) + \frac{F(z-\frac{1}{2}\,\Delta z)\,2\,\pi\,r_{\max}\,\Delta z}{\varrho_{\mathrm{w}}(\bar{T}(z-\frac{1}{2}\Delta z))\,c_{p\mathrm{w}}(\bar{T}(z-\frac{1}{2}\Delta z))\,Q} \tag{50}$$

where Δz represents a positive number, and ϱ_{w} and $c_{p\mathrm{w}}$ stand for the density and the specific heat of water, respectively. Equation (50) is repeatedly applied with Δz corresponding to the lengths of the boundary elements on the cooling surface. The temperature dependent material properties for water at 1 [Bar] are taken from Incropera and De Witt (1990, Table A.6 at page A22). The water temperature at the top of the outer billet surface is assumed to be at 298 [K] with the volumetric flow rate $Q = 6.944 \times 10^{-3}\,[\mathrm{m}^3/\mathrm{s}]$.

The material properties for the Al 4.5 per cent Cu alloy are taken from Pehlke *et al.* (1982) and in contrast to the first case feature the temperature dependence and more realistic liquid fraction – temperature relationship.

The densities of the solid and the liquid phase are assumed to be equivalent with the first test case. The solidus and liquidus temperatures are $T_{\mathcal{S}} = 821.2\,[\mathrm{K}]$, $T_{\mathcal{L}} = 911.0\,[\mathrm{K}]$. The liquid fraction increases between $T_{\mathcal{S}}$ and $T_{\mathcal{L}}$ according to the Sheil law

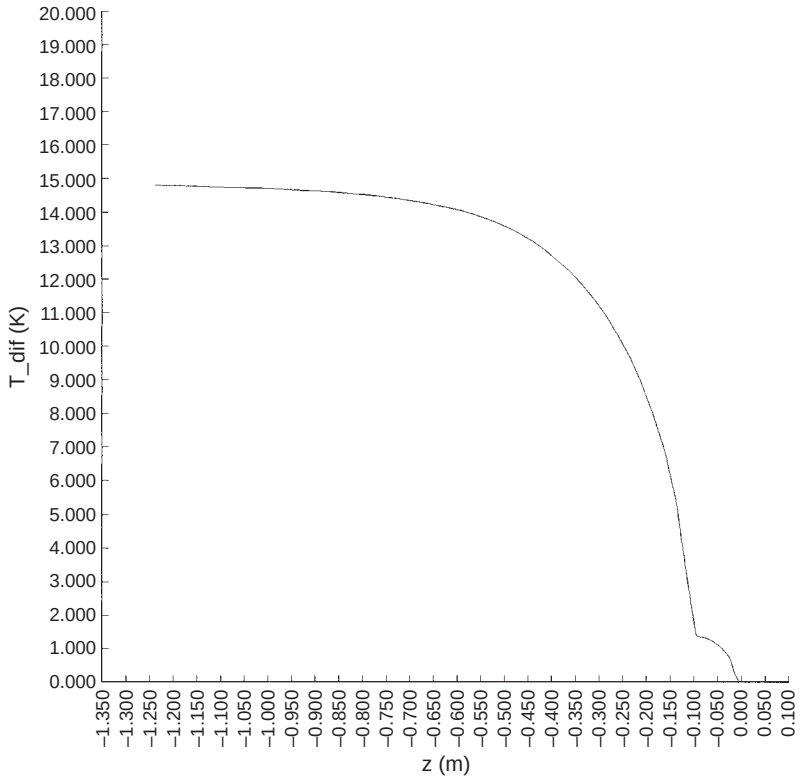

Figure 12.
Second test case. DRBEM results. The increase of cooling water temperature along the billet surface

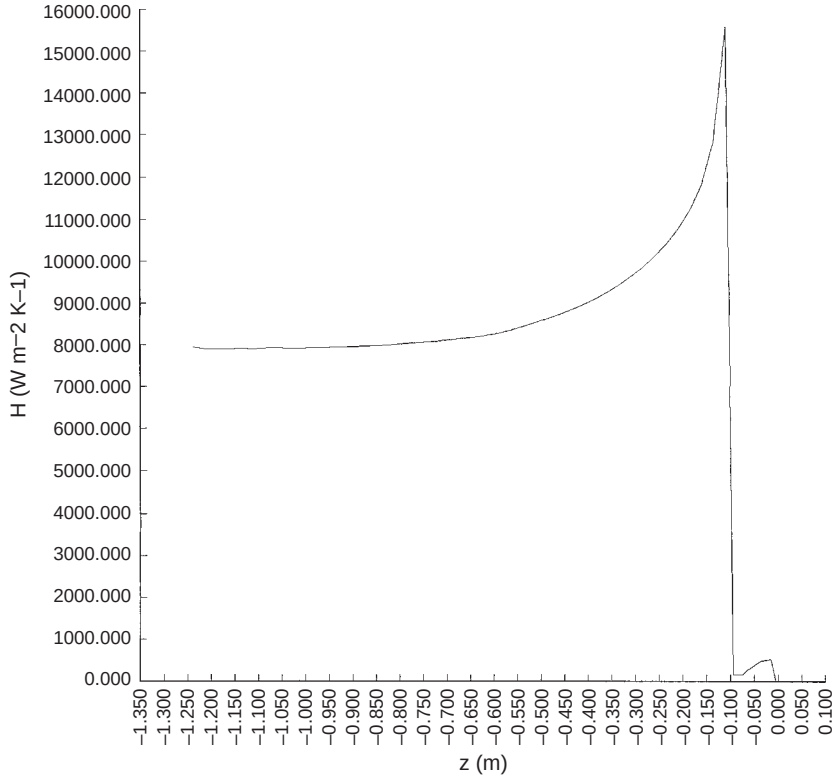

Figure 13.
Second test case. DRBEM results. Heat transfer coefficient distribution along the billet surface

$$f_{\mathcal{L}}(T) = \begin{cases} 0.000 & T \leq T_{\mathcal{S}} \\ (T - ((T_{\mathcal{M}} - T_{\mathcal{S}}^{+})/(T_{\mathcal{M}} - T_{\mathcal{L}}))^{\frac{1}{k_p - 1}})/(T_{\mathcal{S}}^{+} - T_{\mathcal{S}}) & T_{\mathcal{S}} < T < T_{\mathcal{S}}^{+} \\ ((T_{\mathcal{M}} - T)/(T_{\mathcal{M}} - T_{\mathcal{L}}))^{\frac{1}{k_p - 1}} & T_{\mathcal{S}}^{+} < T < T_{\mathcal{L}} \\ 1.000 & T \geq T_{\mathcal{L}}, \end{cases} \tag{51}$$

with $T_{\mathcal{S}}^{+} = T_{\mathcal{S}} + 4\,[\mathrm{K}]$, the melting point of the solvent $T_{\mathcal{M}} = 933.2\,[\mathrm{K}]$, and the equilibrium partition ratio $k_p = 0.17$ (see Figure 9). Melting enthalpy is $H_{\mathcal{M}} = 388837.0\,[\mathrm{J/kg}]$. The thermal conductivity and the specific heat are assumed to be temperature dependent $k_{\mathcal{S}} = k_{\mathcal{L}} = f_k(T)\,[\mathrm{W/(m\,K)}]$, $c_{p\,\mathcal{S}} = c_{p\,\mathcal{L}} = f_{c_p}(T)\,[\mathrm{J/(kg\,K)}]$ and vary as follows

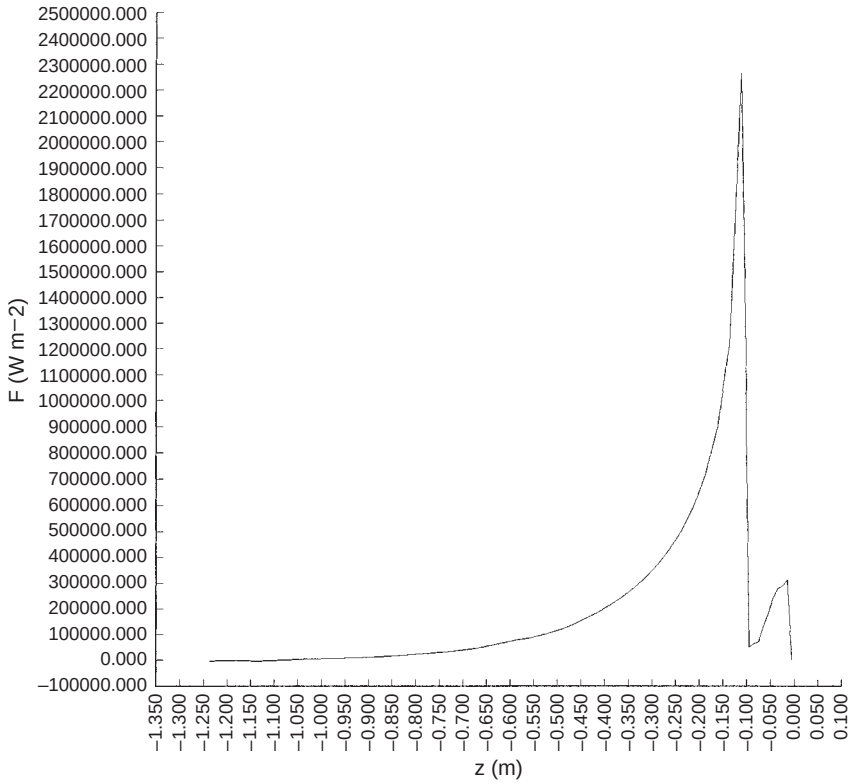

Figure 14.
Second test case. DRBEM results. Heat flux distribution along the billet surface

$$f_k(T) = \begin{cases} 188.300000 & T \leq 523.0\,[\mathrm{K}] \\ 144.368000 + 0.084000 \times T & 523.0\,[\mathrm{K}] < T \leq 573.0\,[\mathrm{K}] \\ 192.500000 & 573.0\,[\mathrm{K}] \leq T \leq 775.0\,[\mathrm{K}] \\ 818.666000 - 0.807956 \times T & 775.0\,[\mathrm{K}] < T \leq 911.0\,[\mathrm{K}] \\ 52.555000 + 0.033000 \times T & T > 911.0\,[\mathrm{K}], \end{cases} \tag{52}$$

$$f_{c_p}(T) = \begin{cases} 748.737000 + 0.0442110 \times T & T \leq 775.0\,[\mathrm{K}] \\ 1286.750000 - 0.2500000 \times T & 775.0\,[\mathrm{K}] \leq T \leq 991.0\,[\mathrm{K}] \\ 1039.000000 & T > 991.0\,[\mathrm{K}], \end{cases} \tag{53}$$

The billet reaches steady-state in 252 timesteps with a maximum of nine and an average of 3.9 internal timestep iterations. The CPU time for the test case is

3,715 seconds. The number of internal timestep iterations is in the second case only slightly different from the first case. The extremely non-uniform mesh used in computations, the temperature dependent material properties and the complex boundary conditions represent no convergence problems. The method in the discussed two examples does not require any over- or under-relaxation, despite the complete non-linear character of the posed problem.

Figure 10 presents the calculated billet temperatures at three radial locations as a function of the axial coordinate. Figure 11 presents the calculated billet isotherms. Figure 12 presents the cooling water temperature increase and Figures 13 and 14 the billet heat transfer coefficient and the heat flux respectively with clearly distinct mould, gap, and direct-chill zones.

5. Conclusions

The present paper demonstrates the successful use of the dual reciprocity boundary element method (Šarler, 1996) for numerical evaluation of physical models that could be previously solved only by more established numerical methods. It probably represents the first industrial use of the boundary element method for solving convective-diffusive phase-change problems with temperature dependent material properties and complex boundary conditions. The essentially new and efficient treatment of the convection term is shown. Scaled axisymmetric thin plate splines have been derived and numerically implemented on a highly non-uniform mesh. The described method was applied in a DC casting simulator of aluminium alloys at the Slovenian company IMPOL Slovenska Bistrica where it was coupled with the process specific mould heat transfer correlations and direct-chill boundary conditions. Excellent agreement was found between the computational model, based on the numerical method described in this paper, and the experimental results. Further research will be focused on upgrades of the method to three-dimensions, iterative solution of the relevant system of algebraic equations, handling of matrix $\mathbf{\Psi}^{-1}$ by iterative techniques, and coupling the treated energy with the momentum equation as formulated in Šarler (1997). The inclusion of the momentum equation will allow us to model the influence of the nozzle and distributor shapes (see Figure 1) which are not taken into account in the present work.

References

Aliabadi, M.H., Beskos, D.E. and Brebbia, C.A. (Eds) (1995), "State-of-the-art on boundary elements and dual/multiple reciprocity techniques", *B.E.Comm.*, Vol. 6, pp. 229-36.

Bennon, W.D. and Incropera, F.P. (1987), "A continuum model for momentum, heat and species transport in binary solid-liquid phase change systems - I. Model formulation", *Int. J. Heat Mass Transfer*, Vol. 30, pp. 2161-70.

Bennon, W.D. and Incropera, F.P. (1988), "Numerical analysis of binary solid-liquid phase change using a continuum model", *Numerical Heat Transfer*, Vol. 13, pp. 227-96.

Bialecki, R., Fic, A., Nowak, A.J. and Wrobel, L.C. (1996), "BEM solution of continuous casting problem", in Wrobel, L.C., Comini, G., Brebbia, C.A. and Nowak, A.J. (Eds), *Advanced Computational Methods in Heat Transfer*, Computational Mechanics Publications, Boston, pp. 337-46.

Brebbia, C.A., Telles, J.C.F. and Wrobel, L.C. (1984), *Boundary Element Techniques; Theory and Applications in Engineering*, Springer-Verlag, Berlin.

Buhmann, M.D. (1990), "Multivariate cardinal interpolation with radial basis functions", *Constr.Approx*, Vol. 6, pp. 225-55.

Bulgakov, V., Šarler, B. and Kuhn, G. (1998), "Iterative solution of systems of equations in the dualreciprocity boundary element method for the diffusion equation", *Int. J. Numer Methods Eng.*

Duchon, J. (1997), "Splines minimizing rotation invariant seminorms in Sobolev spaces", *Constructive Theory of Functions of Several Variables*, Lecture notes in mathematics 571, Springer-Verlag, Berlin, pp. 85-110.

Emley, E.F. (1976), "Continuous casting of aluminium", *Int. Metals Rev.*, pp. 131-89.

Golberg, M.A. and Chen, C.S. (1994), "The theory of radial basis functions applied to the BEM for inhomogenous partial differential equations", *Boundary Elements Comm.*, Vol. 5, pp. 57-61.

Golberg, M.A., Chen, C.S., Bowman, H. and Power, H. (1998), "Some comments on the use of radial basis functions in the dual reciprocity method", *Comp. Mech.*

Incropera, F.P. and De Witt, D.P. (1990), *Fundamentals of Heat and Mass Transfer*, Wiley, New York, NY.

Katgerman, L., Flood, S.C. and Langille, A.H. (1990), "Modelling of D.C. casting of aluminium alloys", in Bouchard, M. and Tremblay, P. (Eds), *Production, Refining, Fabrication and Recycling of Light Metals*, Pergamon Press, New York, NY, pp. 96-110.

Mencinger, J. (1998), "Modeling of heat and momentum transport during melting and solidification", Masters Thesis, University of Ljubljana, Ljubljana.

Ni, J. and Beckermann, C. (1991), "A volume averaged two-phase model for transport phenomena during solidification", *Met. Tran.*, Vol. 22b, pp. 349-61.

Nowak, A.J., Bialecki, R. and Fic, A. (1996), "BEM inverse analysis in thermal problems in continuous and die casting", in Rappaz, M. and Kedro, M. (Eds), *Modelling in Materials Science and Processing*, European Commision, Brussels, pp. 209-19.

Partridge, P.W., Brebbia, C.A. and Wrobel, L.C., (1992), *The Dual Reciprocity Boundary Element Method*, Elsevier, London.

Patankar, S.V. (1980), *Numerical Heat Transfer and Fluid Flow*, Hemisphere, New York, NY.

Pehlke, R.D., Jeyarajan, A. and Wada, H. (1982), *Summary of Thermal Properties for Casting Alloys and Mold Materials*, University of Michigan Technical Report, Ann Arbor, MI.

Powell, M.J.D., (1993), "Some algorithms for thin plate spline interpolation to functions of two variables", *Numerical Analysis Reports*, University of Cambridge, Cambridge.

Press, W.H., Teukolsky, S.A., Vetterling, W.T. and Flannery, B.P. (1992), *Numerical Recipes in Fortran*, Cambridge University Press, Cambridge.

Reddy, A.V. and Beckermann, C. (1997), "Modelling of Macrosegregation due to thermosolutal convection and contraction-driven flow in direct chill continuous casting of an Al-Cu round ingot", *Met. Tran.*, Vol. 28B, pp. 479-89.

Šarler, B. (1996), "Boundary integral formulation of general source-based method for convective-diffusive solid-liquid phase change problems", in Brebbia, C.A., Martins, J.B., Aliabadi, M.H. and Haie, N. (Eds), *BEM-18*, Computational Mechanics Publications, Boston, MA, pp. 551-60.

Šarler, B. (1997), "Dual reciprocity boundary element method formulation of coupled energy, mass and momentum transport in solid-liquid phase change systems", in Van Keer, R. and Brebbia, C.A. (Eds), *Computational Modelling of Free and Moving Boundary Problems*, Computational Mechanics Publications, Southampton, pp. 13-25.

Šarler, B. (1998), "Axisymmetric augmented thin plate splines", *Eng.Anal.*, Vol. 21, pp. 65-79.

Šarler, B. and Kuhn, G., (1998a),"Dual reciprocity boundary element method for convective-diffusive solid liquid phase change problems: Part 1: Formulation", *Eng.Anal.*, Vol. 21, pp. 53-63.

Šarler, B. and Kuhn, G., (1998b), "Dual reciprocity boundary element method for convective-diffusive solid liquid phase change problems: Part 2: Numerical Examples", *Eng.Anal.*, Vol. 21, pp. 65-79.

Šarler, B., Mavko, B. and Kuhn, G. (1993), "Chapter 16: a survey of the attempts for the solution of solid-liquid phase change problems by the boundary element method", in Wrobel, L.C. and Brebbia, C.A. (Eds), *Computational Methods for Free and Moving Boundary Problems in Heat and Fluid Flow*, Computational Engineering Series, Elsevier, London, pp. 737-400.

Voller, V.R., Brent, A.D. and Prakash, C. (1989), "The modelling of heat, mass and solute transport in solidification systems", *Int. J. Heat Mass Transfer*, Vol. 32, pp. 1719-31.

Voller, V.R. and Swaminathan, C.R., (1991), "General source-based method for solidification phase change", *Num. Heat Transfer*, Vol. 19B, pp. 175-89.

Weckman, D.C. and Niessen, P. (1982), "A numerical simulation of the D.C. continuous casting process including nucleate boiling heat transfer", *Met.Trans.*, Vol. 13b, pp. 593–602.

Wrobel, L.C. and Brebbia, C.A. (1987), "The dual reciprocity boundary element formulation for nonlinear diffusion problems", *Comp. Meth. Appl. Mech. Eng.*, Vol. 65, pp. 147-64.

Wrobel, L.C. and DeFigueredo, D.B., (1991), "A dual reciprocity boundary element formulation for convection-diffusion problems with variable velocity fields", *Eng. Anal.*, Vol. 8, pp. 312-19.

Wrobel, L.C. and Telles, J.C.F. (1996), "A dual reciprocity boundary element formulation for axisymmetric diffusion problems", in Brebbia, C.A. and Tanaka, M. (Eds), *BEM-8*, Springer Verlag, Berlin, pp. 59-69.

Wrobel, L.C., Brebbia, C.A. and Nardini, D. (1986), "The dual reciprocity boundary element formulation for transient heat conduction", in Sa da Costa, A., Melo Baptiste, A., Gray, W.G., Brebbia, C.A. and Pinder, G.F. (Eds), *Advances in Water Resources VI*, Springer-Verlag, Berlin, pp. 801-11.

Yamada, T., Wrobel, L.C. and Power, H. (1994), "On the convergence of the dual reciprocity boundary element method", *Eng. Anal.*, Vol. 13, pp. 291-8.